Engineering Shadows to Fabricate Optical Metasurfaces

Engineering Shadows to Fabricate Optical Metasurfaces

A. Nemiroski[1], M. Gonidec[1], J.M. Fox[1], P. Jean-Remy[1], E. Turnage[1], and G.M. Whitesides[1,2,3]*

Abstract: Optical metasurfaces are arrays of plasmonic nanoantennas that resonate at frequencies of 30 – 790 THz, and that can be used to control the properties of scattered light in ways that naturally occurring materials cannot. The difficulty of fabricating these nanostructured composites has slowed the development of planar metamaterials. This paper describes a new technique, Shadow-Sphere Lithography (SSL), that extends nanosphere lithography (NSL) to increase dramatically the range and complexity of structures that can be fabricated. SSL uses software that assembles compositions of shadows to guide multi-angled deposition of one or multiple materials through a self-assembled, colloidal monolayer of plasma-etched microspheres to i) design and fabricate rationally a wide variety of metasurfaces with small features (> 20 nm), complex structures, and/or heterogeneous compositions, and ii) generate, in parallel, many types of structures that enable discovery of new patterns with unexpected optical spectra. The flexibility in design, high areal density of small features, and simplicity of fabrication afforded by SSL make it an end-to-end solution for efficient prototyping and discovery of new, periodic optical metasurfaces.

Keywords: Metamaterials, metasurfaces, flat optics, nanoantennas, plasmonics, nanofabrication, shadow sphere lithography, nanosphere lithography, colloidal lithography, particle lithography.

Affiliations:

[1]Department of Chemistry & Chemical Biology, Harvard University, Cambridge, MA 02138.

[2]Wyss Institute for Biologically Inspired Engineering, Harvard University, Cambridge, MA 02138 USA

[3]The Kavli Insitute for Bionano Science, Harvard University, Cambridge, MA 02138 USA

*Correspondence to: gwhitesides@gmwgroup.harvard.edu.

One Sentence Summary:

Shadow-sphere lithography is a simple method that assembles complex shadow patterns cast by microspheres to fabricate nanoantenna arrays with a wide range of designs and compositions.

Main Text:

Plasmonic metasurfaces (*1-4*)—optically-thin, nanostructured composites that enable the manipulation of light in ways not possible with naturally occurring materials—have the potential to revolutionize photonics by yielding on-chip, planar optical devices [such as frequency-selective surfaces (*5*, *6*); linear and circular polarizers (*7-10*), optical couplers (*11*), beam steerers (*12*), and aberration-free lenses (*6*, *13*, *14*)] with applications to superresolution imaging (*15*), tunable and nonlinear optics (*16*), efficient solar harvesting (*17*), enhanced biosensing (*18*), holography (*19*), optical trapping (*20*, *21*), and analog optical computation (*22*). The exploration of these devices, and the integration of theory and experiment to predict their performance in efficient, functional devices, has been slow, in major part because it has been difficult to fabricate the intricate, finely featured arrays of plasmonic antennas they require, both to collect empirical information and to test theory.

An optical metasurface comprises a two-dimensional (2D), periodic array of conductive nanoantennas (*23*) that couple to incident electromagnetic radiation (and often to one another) via plasmonic resonances (*24*). Theory predicts that this frequency-dependent response can be engineered—by controlling the size, shape, and composition of the antennas, and arrangements of the unit cells in arrays –to manipulate the properties (such as amplitude, phase, and polarization) of scattered light in an almost arbitrary way (*2*, *9*). The only fabrication strategies that permit broad control over appropriate arrays (and then only incompletely) use conventional

photo-, electron-beam, and or ion-beam lithography. These processes, however, are too expensive, too slow in moving from one pattern to another, and too limited in their ability to handle different materials, to be useful in exploration of this field. They are also entirely incompatible with the formation of large numbers of structures semi-randomly. The ability to generate and explore the parameter space of patterns conveniently, empirically, and combinatorially would significantly increase the probability of discovering new optical phenomena.

One attractive alternative to conventional lithography is nanosphere lithography (NSL) (*25*), a convenient methodology that uses monolayer colloidal crystals (MCCs) as stencils to produce fine (> 20 nm), closely-packed, periodic features, over relatively large areas (cm^2). The objective of this paper is to demonstrate that the combination of NSL with the appropriate design software and angled deposition allows for a radical expansion of the spectrum of shadow-derived structures. NSL was originally popularized by Van Duyne (*26*) to fabricate arrays of nanoparticles, and later expanded by use of plasma etching to reduce the diameters of the spheres, and by limited attempts at angled deposition and/or etching to yield simple variations (*27-30*). The convenience of NSL, however, has thus far been limited by the very narrow range of patterns it can produce and the lack of a capability to design new, complex structures.

Here, we show that sequential deposition from multiple angles through a MCC can produce an extensive variety of complex patterns that have not previously been realized physically or considered theoretically. By rationalizing the vast and almost entirely unexplored parameter space of shadow-derived shapes, SSL (Shadow Sphere Lithography) transforms an MCC into a nearly universal stencil. We first demonstrate SSL as a method for rapidly prototyping optical metasurfaces that would be difficult to produce in any other way. We next

explore SSL as a tool for empirical discovery of structures and optical phenomena by investigating a subset of patterns offered by a polycrystalline MCC with thousands of differently oriented domains per cm^2. We finally assess the optical performance of SSL-produced structures by comparing the infrared transmission spectra of a subset of these metasurfaces with the spectra predicted by theory. This work demonstrates SSL to be an operationally simple, generalizable method for fabricating periodic, optical metasurfaces with a wide range of constituent structures and material compositions.

SSL achieves complex deposition patterns by overlapping the shadows cast in a beam of atoms or ions at multiple angles to an MCC. To help visualize these shadows, we first approximated the incident atomic flux by parallel, non-diffraction-limited rays, and modeled the system (spheres, substrate, and sources of projection) in software used for ray tracing (MegaPOV) (*31*). Here, we use the term "projection" to collectively describe physical vapor deposition (PVD), directional etching (such as reactive ion etching, or RIE), or optical ray tracing (in the case of 3D computer rendering). Figure 1A shows how, for a single angle of deposition, the shadows of four, hexagonally non-close-packed (HNCP) spheres can overlap to form an isolated rectangular strip, or "bar". An array of such spheres will, consequently, generate an array of bars. These bars can take on many shapes and positions, which in turn depend on the four free parameters (defined in Figure 1B) of the system: (i) the lattice constant or "pitch", (ii) the width of the "gap" between the spheres, (iii) the polar (inclination) angle θ of the source relative to the MCC, and (iv) the azimuthal (rotation) angle ϕ of the MCC relative to its initial orientation.

For a fixed gap and pitch, and a single source of projection, the morphology of shapes can be tuned by varying θ and ϕ. The shapes that result from different combinations of θ and ϕ

generally belong to a set of five geometrical phases: (1) interconnected lines, (2) asymmetric bars, (3) symmetric bars, (4) triangular islands, or (5) an interconnected, honeycomb-like lattice (Figure S2). Each feature can be duplicated at $\phi = 60^\circ$ intervals due to the six-fold (C_6) rotation symmetry of the hexagonal lattice (Figures 1C-H). Varying the azimuthal angle ϕ produces continuous transitions between the different phases of shadows and offers many intermediate positions and shapes; varying the polar angle θ or the gap between the spheres, controls position, length, and width of each of these features. We discuss this parameter space in the SI

Although ray tracing is a useful tool for modeling shadows, the computation required is too slow to be used for rapid design. To accelerate this process we modeled the shadow of each sphere as an ellipse projected onto the substrate. The positions, orientations, and aspect ratios of these elliptical shadows depend on the free parameters of the system (pitch, gap, and angles of deposition) through simple mathematical relations; multiple angles of deposition can be easily and quickly modeled by overlapping the patterns produced by each individual angle.

Using the aforementioned relations, we developed a Mathematica-based program that composes shadows produced from an arbitrary number of independent angles of deposition (described in the SI). This design environment eliminates the need to consider the abstractions of multi-angled shadows, and makes SSL broadly accessible by allowing users to design structures by "painting" a unit cell. After finalizing a particular design, the software outputs the parameters that are required for fabrication: colloidal diameter, gap, and all angles of projection. Furthermore, we have enabled this software to guide designs that are specified by symmetry only. A user may specify the desired 2D point group (such as C_1, C_2, C_3, C_6, D_1, D_2, D_3, D_6) for a unit cell, and the software suggests patterns with the required symmetries for consideration, further editing, and fabrication (Figure S4).

The range of designs accessible via a HNCP array of spheres suggest that it provides a nearly universal stencil for two reasons: i) the small contact-area of a sphere resting on a flat substrate obscures very little of the underlying substrate from the line of sight associated with some subset of angles, and, thus, most area can be patterned, and ii) the fill-factor of a HNCP array of spheres offers a high areal density of narrow gaps for casting, and overlaying many different shadows. These characteristics enable a sphere-based shadow mask to pattern nearly anywhere within the unit cell (although the gaps available to project patterns are restricted to the p6m symmetry of the array).

In Figure 2, we show patterns composed of two to six different angles of deposition. We first designed these patterns with our Mathematica-based SSL software. We then fabricated MCCs composed of polystyrene spheres with 1-μm diameter at an air/water interface, deposited them on bare silicon wafers, and performed an isotropic etch with oxygen plasma to reduce the diameter of the spheres (*32*), thereby opening the gaps to our design specifications. Finally, we mounted each sample onto a custom-built, dual-axis rotation stage and adjusted the relative angle between the sample and source of deposition, for each angle of deposition, as specified by our designs. Figure 2D characterizes a subset of the experimentally fabricated shapes according to their morphology (connected n-poles, angled resonators, chiral resonators, split dipoles, split-ring resonators, and loop antennas).

One of the major strengths of SSL is the simplicity with which multiple materials can be incorporated into the metasurface without removing the sample from the PVD chamber. This characteristic stands in stark contrast to the time-consuming and costly additional steps (such as registration and additional lithography steps) that would be required to produce such materials with photolithographic methods. Any material that can be deposited by PVD can be used in SSL;

each line segment in a design can correspond to a different material (or thickness of material). Figure 3 demonstrates this capability with patterns composed of three to six different materials. We also include more examples of many other fabricated patterns from one (Figure S7) or multiple materials (Figure S8).

The method of crystallization that we used in this study formed MCCs that contained a large number (~1500/cm^2*)* of hexagonal, single domains with random orientations and areas that ranged from 0 – 25 mm^2. The availability of many large domains (~500 domains/cm^2 with area > 100×100 μm^2) yields many different patterns that can each be optically characterized (SI). This polycrystalline distribution of single domains in a self-assembled MCC simplifies the SSL procedure by eliminating the need to orient samples carefully relative to the initial angle of deposition (the sample provides many correctly oriented domains), and it enables empirical fabrication of new patterns with unexpected structures by providing numerous orientations of domains that differ from those required for the target design. These misaligned domains usually form patterns that are radically different from one another, and each features a unique optical spectrum.

The shapes of misaligned domains provide an important opportunity for the discovery of new metasurfaces, and they can be easily predicted pre-deposition and/or rationalized post-discovery. For example, with a target design that consists of a set of angles of deposition $\{\theta_i, \phi_i\}$ relative to the [100] axis of a chosen domain, the shadows produced within any other randomly oriented domain can be modeled by subtracting an angle ϕ_0—which represents the domain orientation—from the original azimuthal angles (that is, $\{\theta_i, \phi_i\} \rightarrow \{\theta_i, \phi_i - \phi_0\}$). This extra free parameter enables the prediction of all possible structures for a polycrystalline sample;

alternatively, once an interesting pattern is observed, a quick search of the parameter space yields the angular offsets associated with that pattern.

To demonstrate the opportunity for discovery presented by polycrystalline MCCs, we designed an array of four-sided, "looped" nanoantennas (Fig 4A) and investigated a several additional structures formed by misaligned domains (Fig 4B). After fabrication, we used SEM to identify the domains, and Fourier Transform Infrared Spectroscopy (FTIR) to measure their transmission spectra. The shapes produced by these domains could be easily reproduced by the SSL software (Figures 4C-H), and their transmission spectra agreed well with simulations performed by Finite Integration Technique (Figures 4I-N). Although there are thousands of variations in the polycrystalline substrate, all structures belong to three qualitative families (this is evident in Fig. 1C-E as well) due to the C_6 symmetry of the hexagonal lattice. We specifically chose these three examples because they are typical representatives of the three families of shapes and all other domains contains shapes that are intermediate versions of the ones presented.

Two potential complications with SSL are (i) the overlap between shadow-defined features, which cause non-flat topographies, and (ii) the build-up of deposited materials on spheres, which narrows the gaps and, thus, reduces the amount of material that reaches the substrate. Both of these aspects of the technique cause the 3D topology to depart from the idealized flat structures employed in our simulations; however, when simulations were corrected using an "effective thickness" (15 nm) of deposited material, measured and simulated spectra agreed well. The structural distortions caused by non-constant thickness, therefore, appear primarily to shift the entire spectrum slightly (~100 – 200 nm) to the red, and this shift can be accommodated in the simulations via the alteration of a single parameter (the thickness).

SSL allows for the rapid design and fabrication of patterns with a broad range of shapes and material compositions, each of which is equally accessible to simulation and experimental examination. This approach combines nine attributes that make it uniquely useful relative to other strategies for fabricating optical metasurfaces: (i) It can generate closely packed, periodic arrays of complex shapes with small feature sizes (> 20 nm). (ii) It can generate shapes of non-uniform material composition and/or thicknesses. (iii) It allows for rapid fabrication of many optically characterizable domains (500 domain/cm^2 with sizes > 0.01 mm^2 per domain) over large areas (>5 cm^2). (iv) It provides an opportunity for discovery of metasurfaces by providing a continuum of unique variations on designed patterns, each resulting from a different domain orientation. (v) It enables the exploration of the structures that may be specified by symmetries only, and not necessarily by specific designs of the unit cell. (vi) It can easily produce shapes with optically interesting attributes (such as sharp features that yield very strong local electric fields, non-centrosymmetric shapes that couple to linearly polarized light, or chiral shapes that couple to circularly polarized light). (vii) It uses a nearly universal MCC mask that requires a minimum of customization (only plasma etching) and allows designs to be easily scaled up or down simply by changing the size of constituent spheres. (viii) It relies on rapid, easy-to-use, Mathematica-based design software. (iv) It requires a relatively uncomplicated modification to a common commercial system (the installation of a dual-axis rotation stage into an e-beam evaporator). With SSL, the close match between theory and experiment indicates that a simple computer-generated model can be used to predict new structures that are guaranteed to be fabricable and that will behave as expected.

In the future, adjusting angular deposition dynamically (with a computer-controlled rotation stage), or using templated, non-hexagonal patterns and/or non-spherical occluding

objects (such as cubes, which would cast parallelogrammatic shadows) will yield new classes of shapes, wafer-scale domains, gradients in material thickness, and non-periodic arrays. The broad range of complex, multi-material, and multi-thickness nanoantennas afforded by SSL offer new avenues for tuning the optical properties (such as amplitude, polarization, and phase) of metasurfaces that may simplify the exploration of new optical phenomena, such as optical phase gradients that can shape wavefronts (*4*). By bridging the two iteratively linked halves of metasurface development—theory and experiment—this approach promises to accelerate the pace of device design and discovery in the fields of optical metasurfaces, and physical optics.

REFERENCES:

1. A. V. Kildishev, A. Boltasseva, V. M. Shalaev, Planar photonics with metasurfaces, *Science* **339** (2013).
2. C. L. Holloway *et al.*, An overview of the theory and applications of metasurfaces: the two-dimensiona equivalents of metamaterials, *Antennas and Propagation Magazine, IEEE* **54**, 10–35 (2012).
3. N. Yu *et al.*, Flat Optics: Controlling Wavefronts with Optical Antenna Metasurfaces, (2013).
4. N. Yu, F. Capasso, Flat optics with designer metasurfaces, *Nature Materials* (2014).
5. P.-C. Li, Y. Zhao, A. Alù, E. T. Yu, Experimental realization and modeling of a subwavelength frequency-selective plasmonic metasurface, *Applied Physics Letters* **99**, 221106–221106–3 (2011).
6. B. Memarzadeh, H. Mosallaei, Layered plasmonic tripods: an infrared frequency selective surface nanofilter, *Journal of the Optical Society of America B-Optical Physics* **29**, 2347–2351 (2012).
7. T. Ellenbogen, K. Seo, K. B. Crozier, Chromatic plasmonic polarizers for active visible color filtering and polarimetry, *Nano Lett.* **12**, 1026–1031 (2012).
8. Y. Zhao, A. Alù, Manipulating light polarization with ultrathin plasmonic metasurfaces, *Phys. Rev. B* **84**, 205428 (2011).
9. M. A. Kats *et al.*, Giant birefringence in optical antenna arrays with widely tailorable optical anisotropy, *Proceedings of the National Academy of Sciences* **109**, 12364–12368 (2012).
10. N. Yu *et al.*, A broadband, background-free quarter-wave plate based on plasmonic metasurfaces, *Nano Lett.* **12**, 6328–6333 (2012).

11. J. Lin *et al.*, Polarization-Controlled Tunable Directional Coupling of Surface Plasmon Polaritons, *Science(Washington)* **340**, 331–334 (2013).

12. T. Shegai *et al.*, A bimetallic nanoantenna for directional colour routing, *Nature Communications* **2**, 481 (2011).

13. F. Aieta *et al.*, Aberration-free ultrathin flat lenses and axicons at telecom wavelengths based on plasmonic metasurfaces, *Nano Lett.* **12**, 4932–4936 (2012).

14. X. Ni, S. Ishii, A. V. Kildishev, V. M. Shalaev, Ultra-thin, planar, Babinet-inverted plasmonic metalenses, *Light: Science & Applications* **2**, e72 (2013).

15. P.-Y. Chen, A. Alù, Subwavelength imaging using phase-conjugating nonlinear nanoantenna arrays, *Nano Lett.* **11**, 5514–5518 (2011).

16. N. I. Zheludev, Y. S. Kivshar, From metamaterials to metadevices, *Nature Materials* **11**, 917–924 (2012).

17. H. A. Atwater, A. Polman, Plasmonics for improved photovoltaic devices, *Nature Materials* **9**, 205–213 (2010).

18. X. Xu *et al.*, Flexible Visible–Infrared Metamaterials and Their Applications in Highly Sensitive Chemical and Biological Sensing, *Nano Lett.* **11**, 3232–3238 (2011).

19. X. Ni, A. V. Kildishev, V. M. Shalaev, Metasurface holograms for visible light, *Nature Communications* **4** (2013).

20. B. J. Roxworthy *et al.*, Application of plasmonic bowtie nanoantenna arrays for optical trapping, stacking, and sorting, *Nano Lett.* **12**, 796–801 (2012).

21. M. Gullans *et al.*, Nanoplasmonic lattices for ultracold atoms, *Phys. Rev. Lett.* **109**, 235309 (2012).

22. A. Silva *et al.*, Performing Mathematical Operations with Metamaterials, *Science* **343**, 160–163 (2014).

23. A. E. Krasnok *et al.*, Optical nanoantennas, *Physics-Uspekhi* **56**, 539 (2013).

24. V. Giannini, A. I. Fernandez-Dominguez, S. C. Heck, S. A. Maier, Plasmonic nanoantennas: fundamentals and their use in controlling the radiative properties of nanoemitters, *Chem. Rev.* **111**, 3888–3912 (2011).

25. Y. Yu, G. Zhang, Updates in Advanced Lithography, *cdn.intechopen.com* (2013), doi:10.5772/56576.

26. J. C. Hulteen, R. P. Van Duyne, Nanosphere lithography: A materials general fabrication process for periodic particle array surfaces, *Journal of Vacuum Science & Technology A: Vacuum, Surfaces, and Films* **13**, 1553–1558 (1995).

27. A. Kosiorek, W. Kandulski, P. Chudzinski, K. Kempa, M. Giersig, Shadow Nanosphere Lithography: Simulation and Experiment, *Nano Lett.* **4**, 1359–1363 (2004).

28. Y. Choi, S. Hong, L. P. Lee, Shadow overlap ion-beam lithography for nanoarchitectures, *Nano Lett.* **9**, 3726–3731 (2009).

29. J. Zhao, B. Frank, S. Burger, H. Giessen, Large-Area High-Quality Plasmonic Oligomers Fabricated by Angle-Controlled Colloidal Nanolithography, *ACS Nano* **5**, 9009–9016 (2011).

30. N. Vogel *et al.*, Plasmon hybridization in stacked double crescents arrays fabricated by colloidal lithography, *Nano Lett.* **11**, 446–454 (2011).

31. MegaPOV available at http://megapov.inetart.net/.

32. N. Vogel, S. Goerres, K. Landfester, C. K. Weiss, A Convenient Method to Produce Close-and Non-close-Packed Monolayers using Direct Assembly at the Air–Water Interface and Subsequent Plasma-Induced Size Reduction, *Macromolecular Chemistry and Physics* **212**, 1719–1734 (2011).

33. C. L. Haynes, R. P. Van Duyne, Nanosphere lithography: a versatile nanofabrication tool for studies of size-dependent nanoparticle optics, *J. Phys. Chem. B* **105**, 5599–5611 (2001).

34. G. Zhang, D. Wang, H. Möhwald, Fabrication of multiplex quasi-three-dimensional grids of one-dimensional nanostructures via stepwise colloidal lithography, *Nano Lett.* **7**, 3410–3413 (2007).

35. J. Junesch, T. Sannomiya, A. B. Dahlin, Optical Properties of Nanohole Arrays in Metal–Dielectric Double Films Prepared by Mask-on-Metal Colloidal Lithography, *ACS Nano* **6**, 10405–10415 (2012).

36. C. L. Cheung, R. J. Nikolić, C. E. Reinhardt, T. F. Wang, Fabrication of nanopillars by nanosphere lithography, *Nanotechnology* **17**, 1339–1343 (2006).

37. J. Sun *et al.*, Fabrication of centimeter-sized single-domain two-dimensional colloidal crystals in a wedge-shaped cell under capillary forces, *Langmuir* **26**, 7859–7864 (2010).

38. X. Sun, Y. Li, T. H. Zhang, Y.-Q. Ma, Z. Zhang, Fabrication of Large Two-Dimensional Colloidal Crystals via Self-Assembly in an Attractive Force Gradient, *Langmuir* **29**, 7216–7220 (2013).

39. A. D. Rakic, A. B. Djurišic, J. M. Elazar, M. L. Majewski, Optical properties of metallic films for vertical-cavity optoelectronic devices, *Applied optics* **37**, 5271–5283 (1998).

ACKNOWLEDGEMENTS:

We thank N. Vogel, B. Chen, and S. Kostinski for useful discussions. This work was primarily supported by the Office of Naval Research under award no. N00014-10-1-0942 (A.N. and J.M.F). Further support was provided by Marie Curie project SAM-TunEGaIn:IOF-2012-328412 (M.G.); the National Science Foundation (NSF) under award no. DMR-0820484 (E.T.) and DMR-1262895 (P.J.). This work was performed in part at the Center for Nanoscale Systems (CNS), a member of the National Nanotechnology Infrastructure Network (NNIN), which is supported by NSF award no. ECS-0335765. CNS is part of Harvard University. The authors declare no conflict of interest.

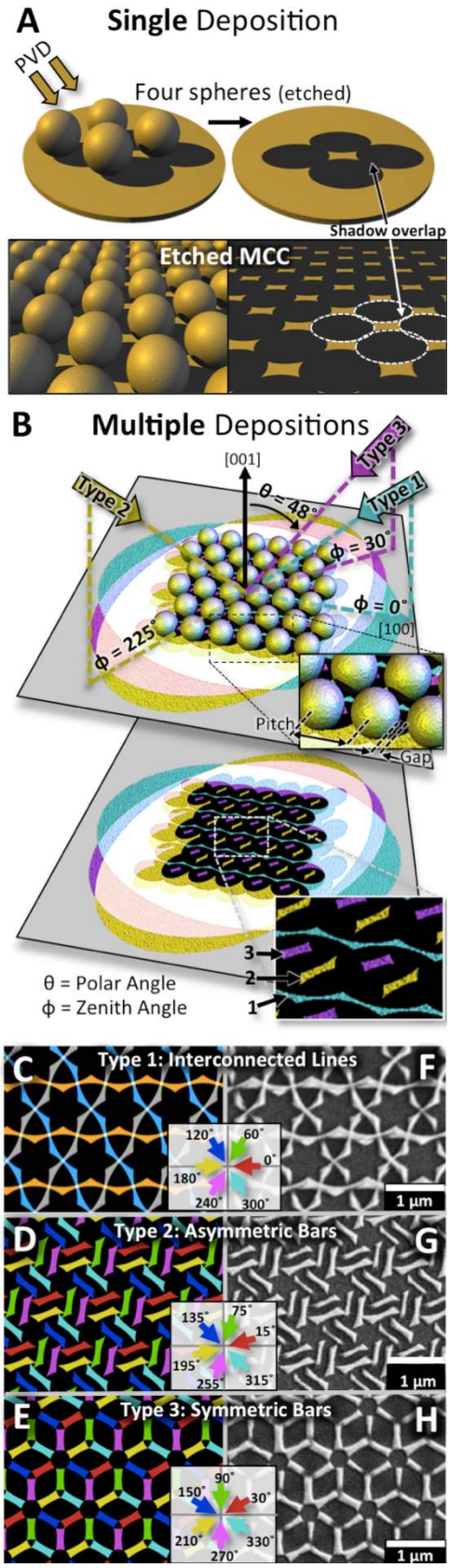
A
Single Deposition
PVD
Four spheres (etched)
Shadow overlap
Etched MCC
B
Multiple Depositions
[001]
Type 3
Type 2
Type 1
θ = 48°
ϕ = 30°
ϕ = 0°
[100]
ϕ = 225°
Pitch
Gap
3
2
1
θ = Polar Angle
ϕ = Zenith Angle
C
Type 1: Interconnected Lines
F
120°
60°
0°
180°
240°
300°
1 µm
D
Type 2: Asymmetric Bars
G
135°
75°
15°
195°
255°
315°
1 µm
E
Type 3: Symmetric Bars
H
90°
150°
30°
210°
270°
330°
1 µm

Figure 1: (A) Generation of a single bar or an array of bars by a single angle of deposition. **(B**) Definition of free parameters relative to the crystal axis. Here we show an example composed of three different types of features: (1) an interconnected line, (2) an asymmetric bar, and (3) a symmetric bar. **(C-E)** A composition of six angles of projection demonstrating the duplication of feature-types 1 – 3 at intervals of $\phi = 60°$ due to the C_6 symmetry of the lattice. **(F-H)** show images collected with a scanning electron microscope (SEM) of the fabricated versions of these patterns (20 nm of Ag on Si). Inset: The six angles by which the features are reproduced.

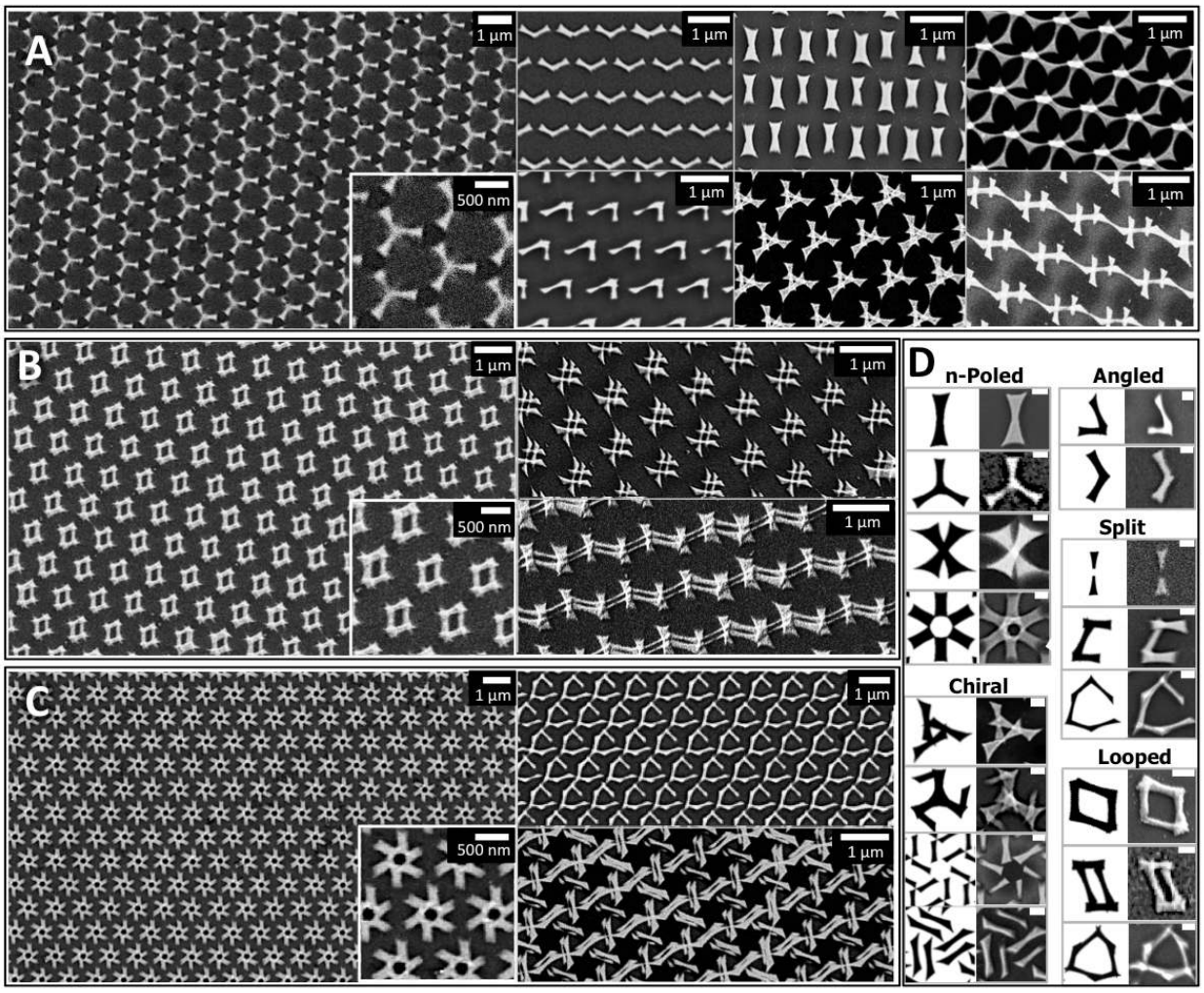

Figure 2: SEM images of various metasurfaces designed and fabricated by SSL composed of **(A)** two to three, **(B)** four, and **(C)** five to six different angles of deposition. **(D)** A subset of possible unit cells categorized according to optical function as designed **(D, Left)** and fabricated **(D, right)**.

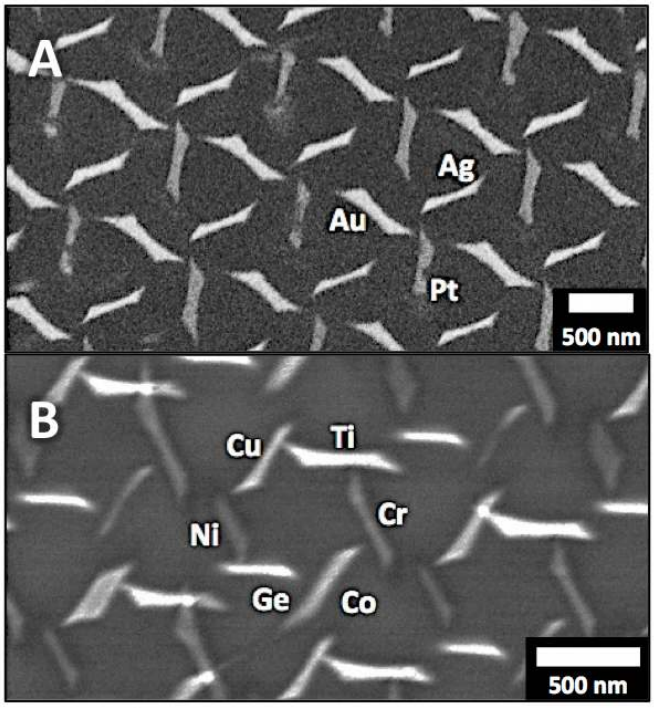

Figure 3: SEM images of **(A)** an array of chiral, tripolar structures (formed by three asymmetric bars) fabricated with each bar composed of 20 nm of either Au, Ag, and Pt, and **(B)** an array of chiral, hexagonal structures (formed by six asymmetric bars) fabricated with each bar composed of 10 nm of either Cu, Ti, Cr, Co, Ge, or Ni.

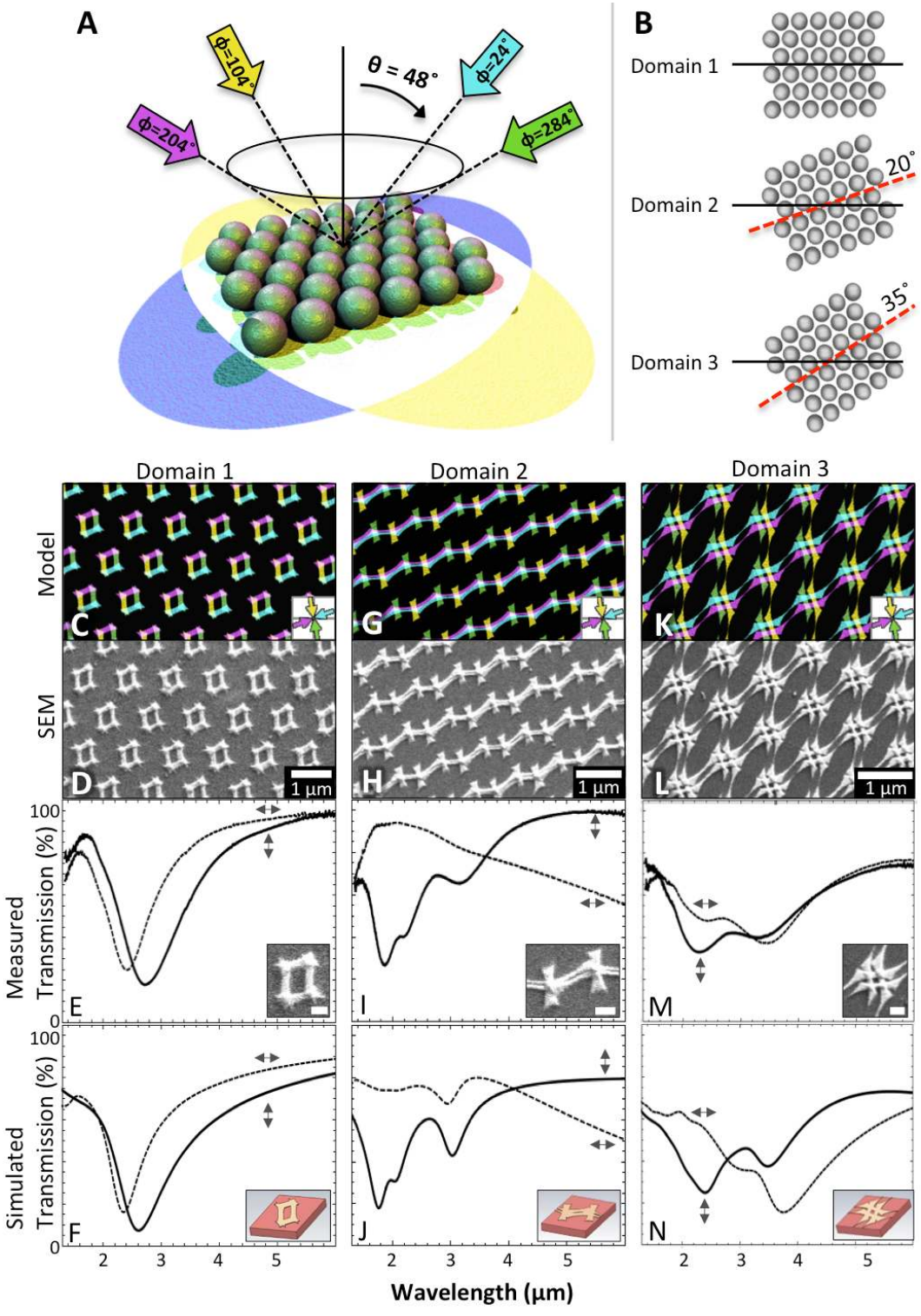
A
ϕ=104°
θ = 48°
ϕ=24°
ϕ=204°
ϕ=284°
B
Domain 1
Domain 2
20°
Domain 3
35°
Domain 1
Domain 2
Domain 3
Model
SEM
C
G
K
D
H
L
1 µm
Measured Transmission (%)
Simulated Transmission (%)
100
0
E
I
M
F
J
N
2
3
4
5
Wavelength (µm)

Figure 4: A comparison of morphology and optical properties between simulated and fabricated metasurfaces on a polycrystalline MCC. **(A)** A 3D scheme for the four angles of deposition used to produce the array of four-sided "looped" array of nanoantennas. We deposited 20 nm of Au onto a borosilicate substrate, through a polystyrene MCC with 1-μm pitch and 120-nm gap. **(B)** The orientation (relative to the initial design) of three domains on the same substrate that we chose to characterize. **(C-E)** The modeled domains. **(F-H)** SEM images of the fabricated domains. **(I-K)** FTIR transmission spectra of the fabricated domains. The incident polarization is labeled near each spectrum. Scale bars on the inset figures represent 200 nm. (**L-N**) Simulated transmission spectra. Inset figures show the simulated unit cells.